



OPEN

# Enhanced transparency, mechanical durability, and antibacterial activity of zinc nanoparticles on glass substrate

SUBJECT AREAS:  
NANOPARTICLES  
SYNTHESIS AND PROCESSINGReceived  
16 May 2014Accepted  
5 August 2014Published  
3 September 2014Correspondence and  
requests for materials  
should be addressed to  
S.-G.Y. (sgyoon@cnu.  
ac.kr)Hyung-Jin Choi<sup>1</sup>, Jin-Seok Choi<sup>2</sup>, Byeong-Ju Park<sup>1</sup>, Ji-Ho Eom<sup>1</sup>, So-Young Heo<sup>1</sup>, Min-Wook Jung<sup>3</sup>,  
Ki-Seok An<sup>3</sup> & Soon-Gil Yoon<sup>1</sup>

<sup>1</sup>Department of Materials Engineering, Chungnam National University, Daeduk Science Town, 305-764, Daejeon, Korea, <sup>2</sup>Research Analysis Center, Korea Advanced Institute of Science and Technology, 291 Daehak-ro, Yuseong-gu, 305-701, Daejeon, Korea, <sup>3</sup>Thin Film Materials Research Group, Korea Research Institute of Chemical Technology, 19 Sinseongno, Yuseong-gu, Daejeon 305-600, Korea.

Homogeneously distributed zinc nanoparticles (NPs) on the glass substrate were investigated for the transmittance, mechanical durability, and antibacterial effect. The buffered Ti NPs between Zn NPs and glass substrate were studied for an enhancement of the transmittance and mechanical endurance. The Ti NPs buffered Zn NPs showed a high transmittance of approximately 91.5% (at a wavelength of 550 nm) and a strong antibacterial activity for *Staphylococcus aureus* and *Escherichia coli* bacteria. The buffered Ti NPs are attractive for an excellent mechanical endurance of the Zn NPs. The Zn NPs did not require the protection layer to prevent the degradation of the performance for both the antibacterial effect and the transmittance.

The prevention of microbial surface contamination has become most crucial in today's health care system, and in food and pharmaceutical production. Human beings are often infected by microorganisms such as bacteria, viruses, and molds that often infect living environments. Silver nanoparticles or silver ions have been known to have strong inhibitory and bactericidal effects<sup>1-9</sup>. Metallic nanoparticles are most promising as they show good antibacterial properties due to their large surface area to volume ratio, which is coming up as the current interest in the researchers due to the growing microbial resistance against metal ions, antibiotics and the development of resistant strains<sup>7</sup>. However, although the silver NPs showed a good antibacterial effect, they exhibited a strong toxicity to humans and a high cost for mass-production. Recently, transparent electronic devices were widely used as the electronic devices were integrated onto the glass panels. All of electronic devices were required to be applied for the antibacterial function, keeping a high transparency comparable to the glass panels. In addition, the mechanical durability of the glass panels with an antibacterial effect is required for long-term applications.

Most of the reported results were mainly focused on the zinc oxide nanoparticles for antibacterial effect<sup>10-13</sup>. However, zinc oxide nanoparticles were mainly prepared by solution technique, which resulted in an inhomogeneous antibacterial effect due to the severe agglomeration of the nanoparticles. Zinc oxide nanoparticles are very difficult to establish the comparable transmittance to the glass substrate. Compared with silver NPs, zinc showed no toxicity to humans and a low-cost for mass-production. If the Zn NPs grown on the glass substrate exhibited an antibacterial activity and a comparable transmittance to the glass, because they were easily oxidized in air atmosphere for a long time and then changed to ZnO NPs, they were expected to be exhibited an antibacterial performance and a comparable transmittance to the glass substrate.

To the best of our knowledge, the study to enhance both the transmittance and the antibacterial property using pure zinc NPs has not been reported. In the present study, zinc NPs instead of silver were chosen for antibacterial function and their influence on the transmittance was investigated using samples deposited by optimum conditions. For enhanced mechanical endurance of the zinc NPs on glass substrate, the Ti NPs were used as an adhesion layer between zinc NPs and glass. The reason that the Ti NPs deposited via a physical vapor deposition (PVD) process exhibited such a strong adhesion with the glass substrates was intensively investigated in the present study. Morphology, transmittance, antibacterial effect, and mechanical endurance of the zinc NP/glass was investigated for different structures such as Zn NPs/glass, Zn NPs/SiO<sub>2</sub>/glass, and Zn NPs/Ti NPs/glass.



## Results

Characterization of the SiO<sub>2</sub> film and the Ti NPs as buffer layers is interesting for the deposition of zinc NPs onto the glass substrate because the Zn NPs showed a weak adhesion with the glass substrate. Figures 1(a) and 1(b) showed variations in transmittance of 15 nm-thick SiO<sub>2</sub> films/glass and Ti NPs/glass as a function of wavelength, respectively. The inset at each figure showed an enlarged transmittance to clearly identify the difference between buffer layers/glass and bare-glass substrate. Transmittance of the 15 nm-thick SiO<sub>2</sub> buffer layer showed a decrease of approximately 0.4% at a wavelength of 550 nm, compared with the transmittance of glass, as shown in Figure 1(b). On the other hand, the Ti NPs/glass showed a consistent transmittance with that of the glass substrate, which showed in an enlarged transmittance (an inset). For determination of the optimum deposition conditions of the Ti NPs, SEM surface images of the Ti NPs deposited onto the glass substrate at different dc powers and for different deposition times were shown in Fig. S1 (Supplementary Information). Based on the transmittance and SEM surface images, dc power of 20 W for 40 s was an optimum condition for the deposition of Ti NPs. Figure 1(c) and 1(d) showed SEM surface image of the SiO<sub>2</sub>/glass and Ti NP/glass, respectively. The 15 nm-thick SiO<sub>2</sub> films showed smooth morphologies with a root mean square (rms) roughness of 0.12 nm (Fig. 1(c)). On the other hand, Ti NPs deposited on the glass showed homogeneously distributed particles with rms roughness of approximately 0.36 nm (Fig. 1(d)). Their average particle sizes were approximately 10–20 nm. Based on the transmittance and the homogeneous morphologies of the Ti NPs, the buffered Ti NPs were expected not to influence the transmittance of the zinc NPs deposited on the glass substrate.

## Discussion

Figure 2(a) shows the relationship between transmittance and the wavelength of the Zn NPs deposited on the glass substrate for different times at a dc power of 8 W. The Zn NPs deposited for 40 and 60 s showed a comparable transmittance (~91.5% at a wavelength of 550 nm) to the bare glass substrate, while transmittance of the samples deposited for above 70 s abruptly decreased in the range of visible wavelength. Based on the SEM surface images of the Zn NPs deposited for 40 (Fig. 2 (b-1)) and 80 s (Fig. 2 (b-2)), Zn NPs were confirmed to be clearly formed on the glass substrate. The average particle size of the samples shown at (b-1) and (b-2) was approximately 17 and 30 nm, respectively. The relationship between the particle size and the wavelength of the incident beam was reported by Ahn et al.<sup>14</sup>. In the present study, UV/VIS/NIR spectrometer used to study the optical properties of the samples was consisted of photomultiplier tube (PMT) detectors. The PMT detector only captures light transmitted in the same direction as the incident light. Transmittance spectra from the PMT detector were averaged at 400–800 nm wavelength range. The mean particle sizes of the Zn NPs were determined through the SEM surface image of the Zn NPs deposited for different times at dc power of 8 W. Based on the relationship between average transmittance and particle size (Fig. 2(c)), average transmittance was maintained at approximately 91.6% at a mean particle size of 23 nm, while it decreased with increasing particle size above 27 nm. Dependence of the transmittance on the particle size was explained using anti-reflection, diffraction, and diffusive scattering for 0.14–0.2 μm, 0.5–4 μm, 5–10 μm, respectively<sup>14</sup>. However, in the present study, the average particle size was below 40 nm. The reason for such size dependence is presently not

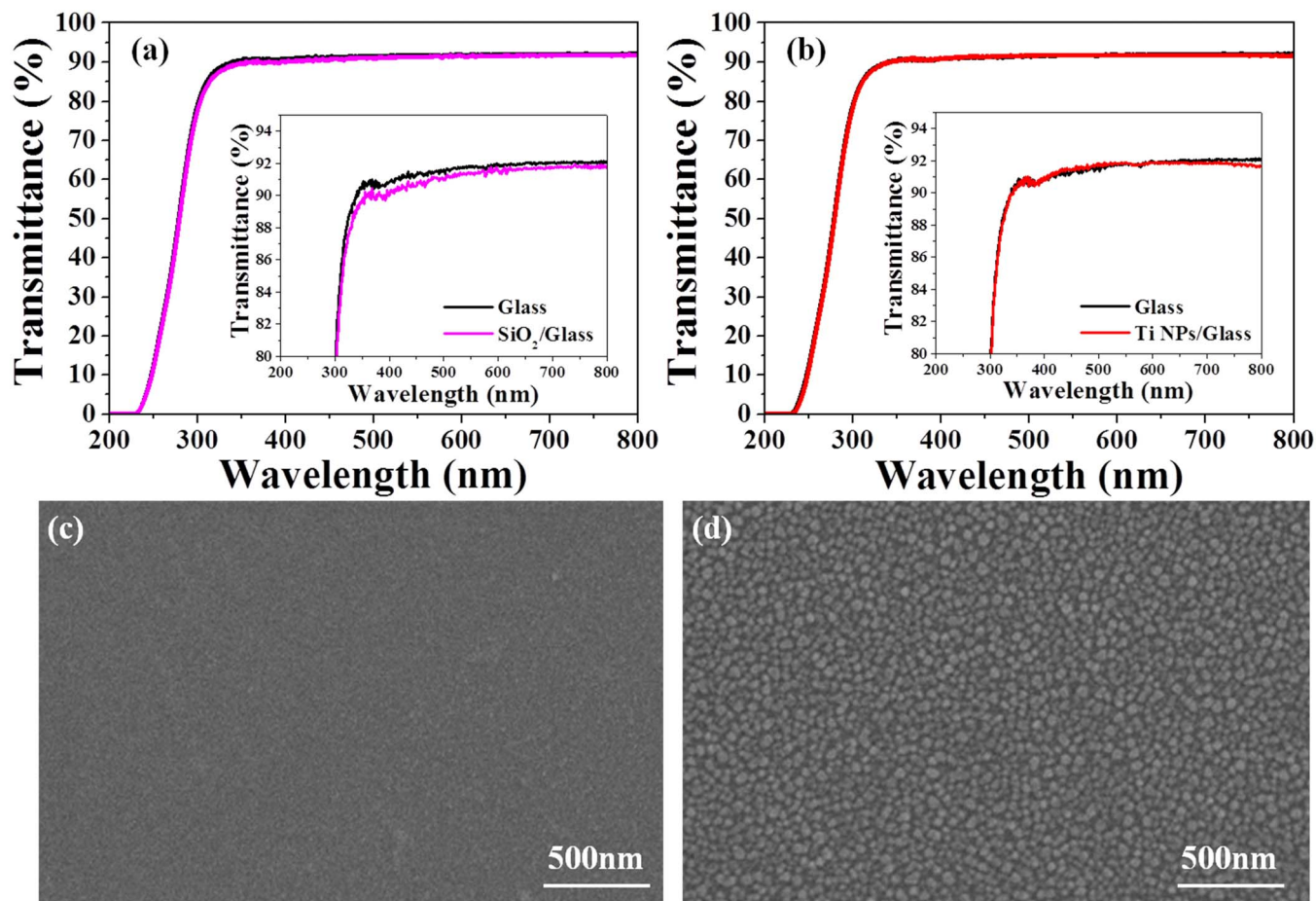


**Figure 1** | Variations in transmittance of (a) 15nm-thick SiO<sub>2</sub> films/glass and (b) Ti NPs/glass as a function of wavelength. SEM surface image of (c) the SiO<sub>2</sub> film and (d) Ti NPs deposited on the glass substrate.

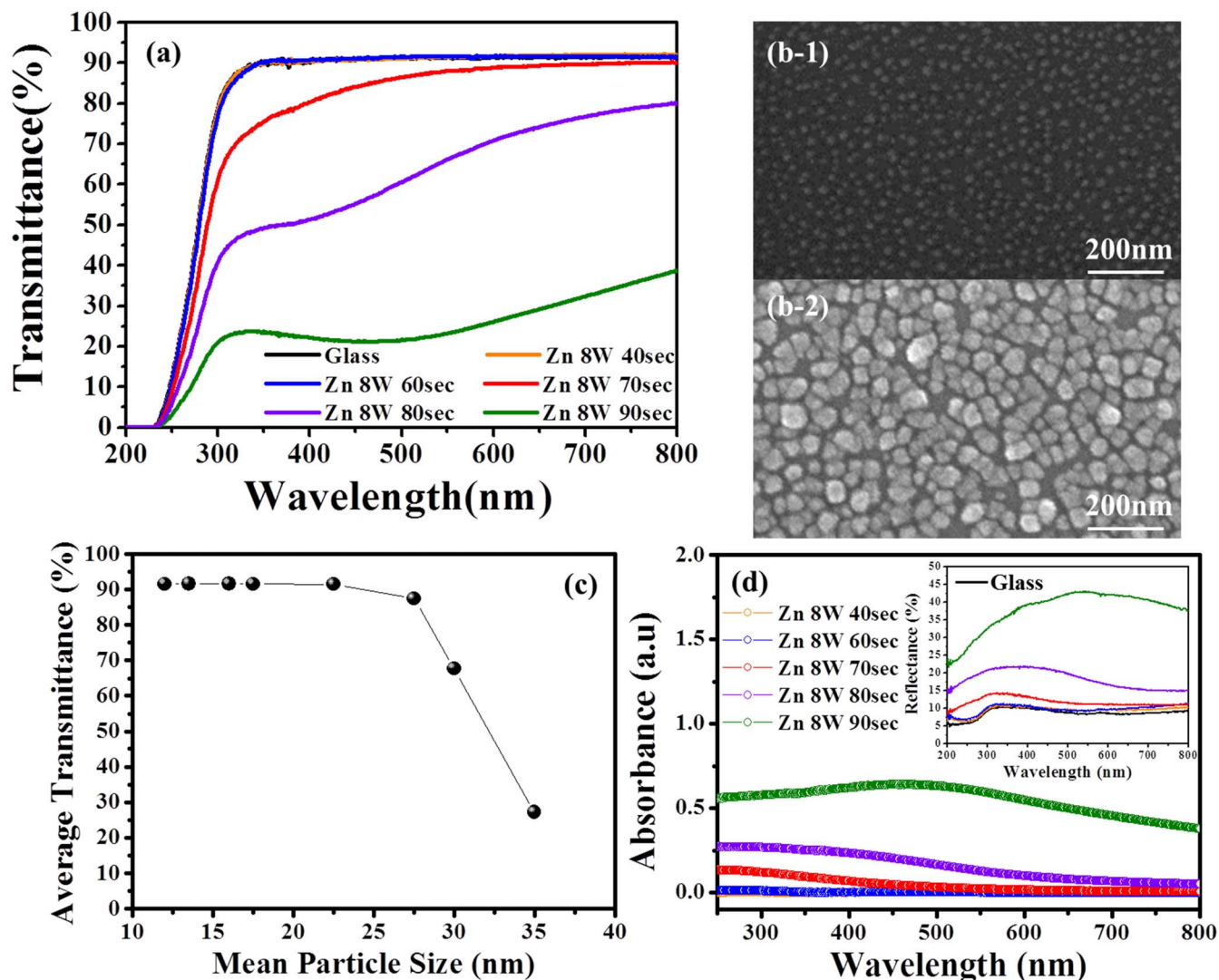


**Figure 2** | (a) Relationship between transmittance and the wavelength of the Zn NPs deposited for various times on the glass substrate at a dc power of 6 W. (b) SEM surface images of the Zn NPs deposited for ((b-1)) 40 and ((b-2)) 80 s. (c) The relationship between average transmittance and mean particle size. (d) Relationship between absorbance and wavelength for Zn NPs prepared for different deposition times. Inset of (d) showed the relationship between reflection and wavelength for Zn NPs prepared for different deposition times.

clearly understood. Although the anti-reflection was observed when the particle size is around a quarter of the wavelength of the incident visible light, particle size below 40 nm was still expected to be observed by an anti-reflection. The relationship between absorbance and wavelength for Zn NPs prepared for different deposition times (Fig. 2(d)) showed that the Zn NPs deposited for 40 and 60 s showed no absorbance in the range of wavelength from 300 to 800 nm. On the other hand, Zn NPs grown for 70 to 90 s showed an increase of the absorbance. The tendency of the variations in the reflectance (inset of Fig. 2(d)) is consistent with those of transmittance and absorbance. Based on the results of transmittance, deposition condition of the Zn NPs with approximately 15–20 nm sizes was established at a dc power of 8 W for 40 s.

Figure 3 showed SEM surface images and transmittances of Zn NPs/glass, Zn NPs/Ti NPs/glass, and Zn NPs/SiO<sub>2</sub>/glass. From the SEM surface images, Zn NPs showed the dense and homogeneous distributions on the bare-glass (Fig. 3(a)), Ti NPs/glass (Fig. 3(b)), and SiO<sub>2</sub>/glass (Fig. 3(c)). Particle sizes of the Zn NPs were in the range of approximately 12–18 nm. Variations in transmittance of the Zn NPs grown onto the various buffer layers were shown in Figure 3(d) and an inset showed an enlarged transmittance for different buffer layers. Compared with the transmittance of the bare-

glass (91.7% at a wavelength of 550 nm), transmittances of the Zn NPs/glass, Zn NPs/Ti NPs/glass, and Zn NPs/SiO<sub>2</sub>/glass were approximately 91.5, 91.5, and 90.3%, respectively, at a wavelength of 550 nm. A remarkable decrease of the transmittance of the Zn NPs/SiO<sub>2</sub>/glass was attributed to the decrease of the transmittance by the SiO<sub>2</sub> buffer layer (see Fig. 1(a)). The decrease in transmittance of the SiO<sub>2</sub>-coated glass substrate, as compared with that of bare-glass was consistent with the reported result<sup>15</sup>. The sheet resistances of the Zn NPs deposited on the various buffer layers were approximately  $1.5 \pm 0.1 \times 10^8 \Omega/\text{square}$ , compared with that of the bare-glass ( $1.6 \times 10^8 \Omega/\text{square}$ ). The results suggested that the Zn NPs exhibiting an insulating property did not influence the electronic performance of the Zn NP-based electronic devices.

Mechanical durability of the Zn NPs grown onto the various buffer layers was performed at the repeated 2,000 swipes. Based on the variations in transmittance and surface image after swipes of the Zn NPs grown on the various buffer layers (Fig. 4(a)), transmittance of the Zn NPs/glass after 2,000 swipes showed a decrease of about 1.3%, compared with that of no swipe, and the SEM image showed a partial removal and an agglomeration of the Zn particles (see Fig. 4(d)). The result suggested that the Zn NPs had an adhesion problem with bare-glass substrate. On the other hand, transmittance

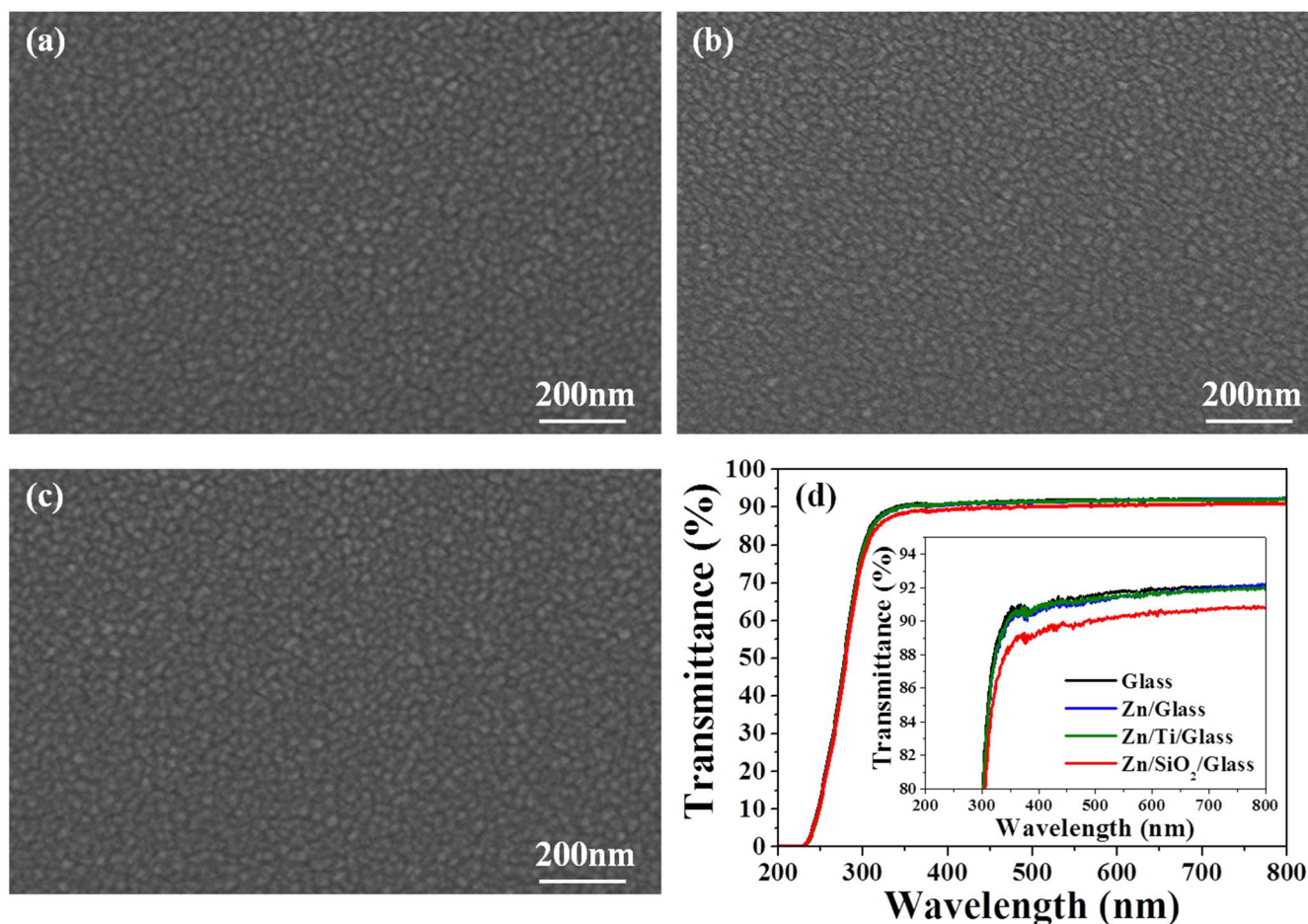


**Figure 3** | SEM surface image of (a) Zn NPs/glass, (b) Zn NPs/Ti NPs/glass, (c) Zn NPs/SiO<sub>2</sub>/glass. (d) Relationship between transmittance and wavelength of Zn NPs/glass, Zn NPs/SiO<sub>2</sub>/glass, and Zn NPs/Ti NPs/glass. Inset of (d) showed an enlarged transmittance for above 80%.

of the Zn NPs/SiO<sub>2</sub>/glass (Fig. 4(b)) and Zn NPs/Ti NPs/glass (Fig. 4(c)) showed a decrease of only 0.5 and 0.4%, respectively, after 2,000 swipes. SEM images of the Zn NPs/SiO<sub>2</sub>/glass (Fig. 4(e)) and Zn NPs/Ti NPs/glass (Fig. 4(f)) observed after 2,000 swipes definitely showed that the Zn NPs still remained like as-deposited Zn NPs although they received a small damage in the case of the Zn NPs/SiO<sub>2</sub>/glass. Contrary to the Zn NPs/glass, Zn NPs/SiO<sub>2</sub>/glass and Zn NPs/Ti NPs/glass showed a small damage by swipes, indicating a slight agglomeration of the particles. The agglomeration of the NPs at several places by the swipes influenced a slight decrease of the transmittance. However, transmittance of the Zn NPs/Ti NPs/glass was still remained above 91% after 2,000 swipes. The Zn NPs are directly contacted with Ti NPs. The Ti and Zn NPs have a large surface area, indicating a large surface energy of the NPs. Therefore, the Zn NPs are reacted with the Ti NPs to reduce the surface energy, resulting in a strong bonding. The Ti NPs for the strong adhesion of the Zn NPs on the glass substrate are suitable for applications in the glass panels of the electronic devices. Actually, in the physical vapor deposition (PVD) such as dc or radio-frequency sputtering, adhesion between the deposited materials and substrate was attributed to the mechanical entanglement of the atoms. The bonding force by a mechanical entanglement is weaker than that by the chemical reaction between the deposited material and the substrate. Nevertheless, titanium deposited by PVD is often used as the adhesion layer between a metal electrode and the arbitrary substrates<sup>16–18</sup>. However, to the best of our knowledge, the reason that titanium shows such good adhesion with substrates remains unreported. To examine the adhesion characteristics of the titanium, an interface state between Ti layer and glass substrate was analyzed by

X-ray photoelectron spectroscopy (XPS) using the 50 nm-thick Ti film deposited on the glass substrate at room temperature under argon atmosphere. The survey spectra observed after etching for different times were shown in Fig. 5(a). The survey spectrum of the Ti surface (for 0 sec, no etching) showed Ti and carbon peaks only (at a binding energy of 285 eV). The removal of the carbon peak in sample etched for 100 s means the carbon contaminated from the sample handling. The Si 2P, 103 eV and Si 2S, 151 eV peaks observed in samples etched at 700 s are those of the SiO<sub>2</sub> that is main composition of the glass substrate. This means that the etching for 700 s exhibits the interface between Ti and glass substrate. Therefore, Ti 2P core level in an interface etched at 700 s was investigated in detail (Fig. 5(b)). The phases observed through the optimum fitting processes of Ti 2p core level were Ti, TiO, TiO<sub>2</sub>, Ti<sub>2</sub>O<sub>3</sub>, and Ti<sub>3</sub>O<sub>5</sub>. The titanium oxide phases except Ti were formed by a chemical reaction between Ti and O originated from the glass substrate. By the preferential thermodynamic expectation, Gibbs-free energies of the TiO, TiO<sub>2</sub>, Ti<sub>2</sub>O<sub>3</sub>, and Ti<sub>3</sub>O<sub>5</sub> phase, which are possible phases by a chemical reaction between Ti and O, are  $-509.5$ ,  $-862.1$ ,  $-713.6$ , and  $-769.8$  kJ, respectively, at 300 K<sup>19</sup>. Titanium oxide phases had the lowest Gibbs-free energies, as compared with the other titanium compounds such as halides, sulphides, nitrides, and silicides. The actual observation of the titanium oxide phases formed by a chemical reaction between Ti and O originated from the glass substrate was consistent with the thermodynamic expectation. As a result, the strong adhesion between Ti and glass substrate was attributed to the chemical bonding by a chemical reaction with Ti and O from the glass substrate. However, in Zn NPs/Ti NPs/glass samples, it is very important to observe the antibacterial effects of the Ti NPs only

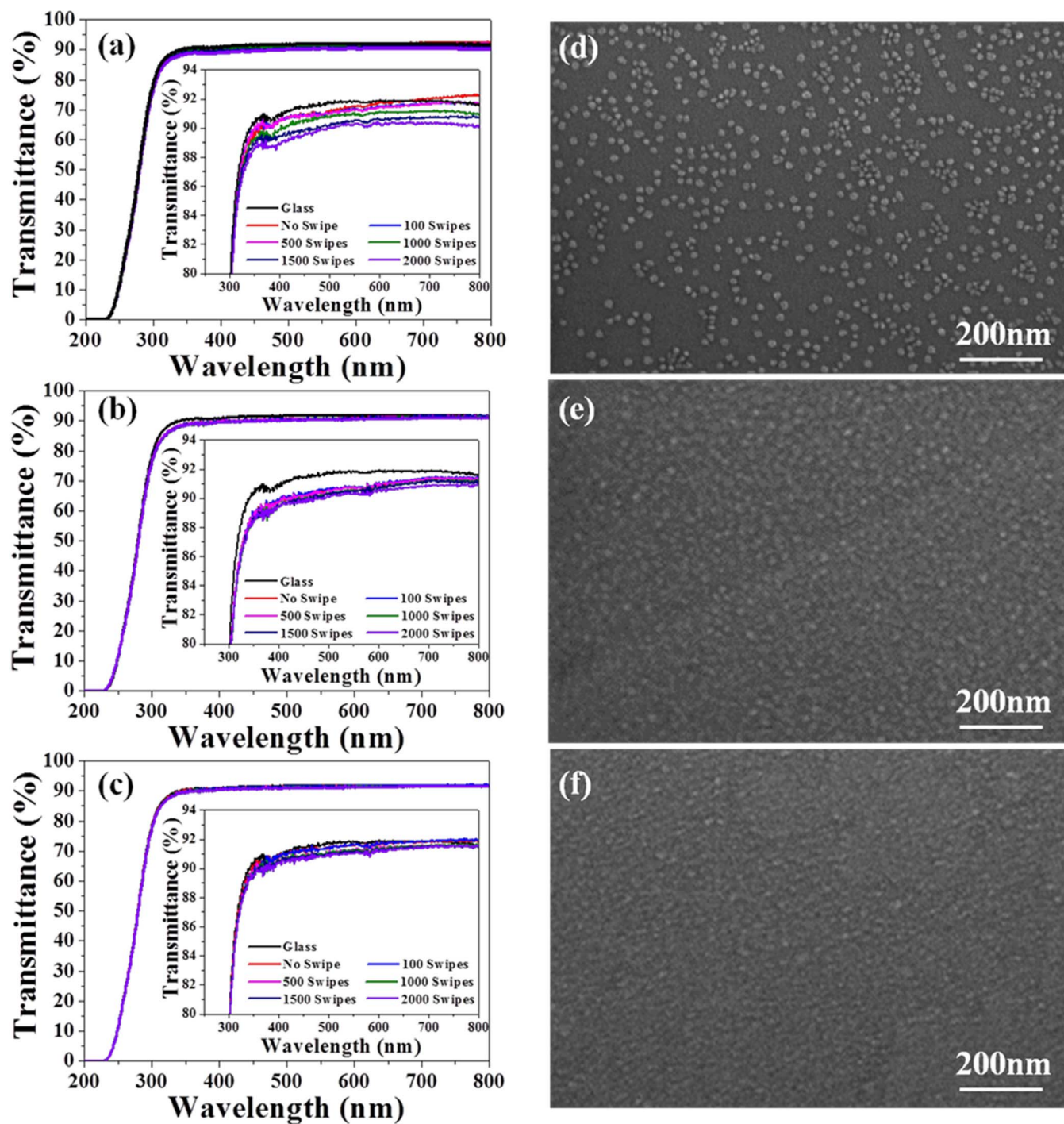


**Figure 4** | Variations in transmittance after swipes using the Zn NPs grown on the (a) glass, (b) SiO<sub>2</sub>/glass, and (c) Ti NPs/glass substrate. (d), (e), and (f) SEM surface images measured after 2,000 swipes using (a), (b), and (c) samples, respectively. Insets in (a), (b), and (c) figure showed an enlarged transmittance for above 80%.

because the Ti NPs should only be played an important role as the adhesion characteristics. Accordingly, in the present study, antibacterial effects of the Ti NPs/glass including the Zn NPs/SiO<sub>2</sub>/glass, and the Zn NPs/Ti NPs/glass were analyzed using *Staphylococcus aureus* (*S. aureus*) and *Escherichia coli* (*E. coli*) bacteria by a film attachment method. Figure 6(a) shows the actual images of the *S. aureus* and *E. coli* after incubation for 24 h. Figures 6(a-1) and 6(a-5) showed the actual images of the incubated *S. aureus* and *E. coli*, respectively, without zinc-NPs (blank). Figures 6(a-2) and 6(a-6) showed the actual images of the incubated *S. aureus* and *E. coli*, respectively, using Ti NPs/glass. The number of the bacterial was decided by the

counts of colonies, which described in p. 10 of JIS (Japanese Industrial Standard) Z 2801<sup>20</sup>. The number of viable bacteria (N) is calculated as follows:<sup>20,21</sup>

$$N = C \times D \times V \quad (1)$$

Where C is the number of colonies; D is the dilution ratio and V is the volume of neutralizer broth used to detach bacteria. As shown in Fig. 6(a-2) and 6(a-6), the number of *S. aureus* was decreased and the number of *E. coli* was increased after an incubation, compared with those of the blank. This result suggested that the Ti NPs did not

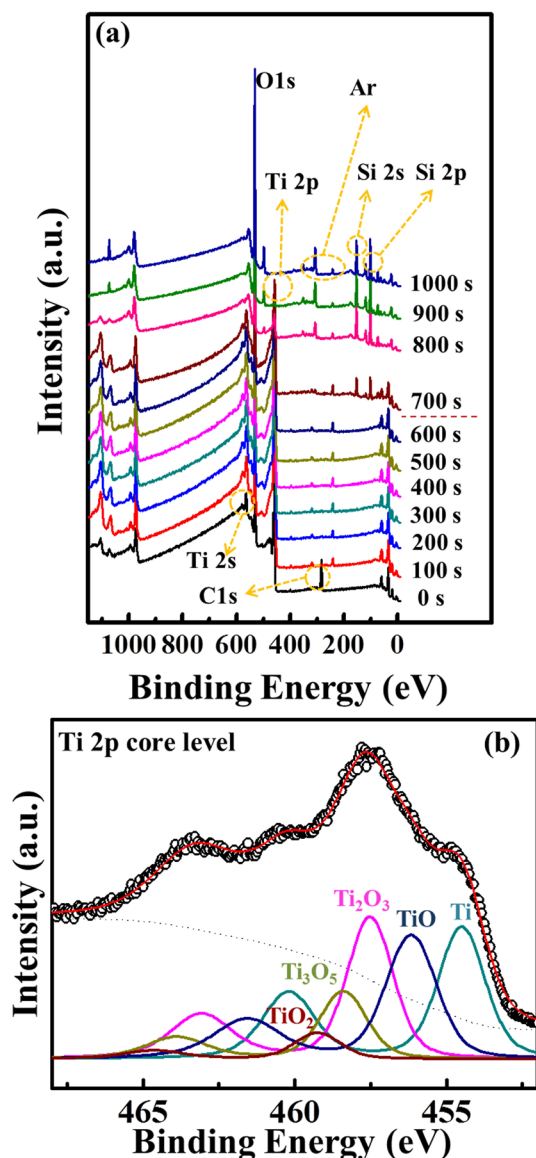


**Figure 5** | (a) Survey XPS spectra for different etching times from the Ti surface using the Ti (50 nm)/glass substrate. (b) Ti 2p core level observed at an interface between the Ti film and the glass substrate after an etching for 700 s. Fitting curves showed different phases observed at an interface between the Ti film and the glass substrate.

contribute to the reduction of the bacteria, indicating no antibacterial effect. However, in the case of Zn NPs/SiO<sub>2</sub>/glass (a-3, a-7) and Zn NPs/Ti NPs/glass (a-4, a-8), no bacteria were observed after an incubation. Table 1 summarized the antibacterial test results after 24 h incubation against *S. aureus* and *E. coli* using samples of Ti NPs/glass, Zn/SiO<sub>2</sub>/glass, and Zn NPs/Ti NPs/glass. Table 1 includes the test results using samples of Zn NPs/Ti NPs/glass maintained for 3 months in air atmosphere at room temperature. In the case of Zn NPs and Zn NPs/Ti NPs, the percent reductions of bacteria were 99.99668% and 99.99999% against *S. aureus* and *E. coli*, respectively. In samples maintained for 3 months, percent reductions of the bacteria were noticeably observed. This result suggested that the antibacterial effect of the Zn NPs/Ti NPs/glass exhibited a long-term stability in a natural state. The present result was comparable to that reported in the case of silver NPs by Lee *et al.*<sup>22</sup>.

Figure 6(b) shows the antibacterial activity of the Ti NPs/glass, Zn NPs/SiO<sub>2</sub>/glass, Zn NPs/Ti NPs/glass, and Zn NPs/Ti NPs/glass maintained for 3 months in a natural state. The efficacy of anti-

microbial products was judged from the value of antibacterial activity. Antibacterial activity was obtained as follows: Antibacterial activity = log (the number of bacteria counted after the incubation of bacteria for 24 h onto the bare glass (blank)) – log (the number of bacteria counted after the incubation of bacteria for 24 h onto the Zn NPs). The value of antibacterial activity obtained by the testing methods of this standard should not be less than 2.0 for the antibacterial efficacy of antibacterial products<sup>20</sup>. Values of over 2.0 may be applicable subject to the agreement between parties concerned with delivery. In the present study, for reliability of the antibacterial activity, it was obtained by averaging the values measured using six samples for each *E. coli* and *S. aureus* bacteria. The antibacterial activity of the Ti NPs/glass was below 2.0 for *E. coli* and *S. aureus*. The result suggested that the Ti NPs did not exhibit the antibacterial effect. On the other hand, The Zn NPs/SiO<sub>2</sub>/glass, Zn NPs/Ti NPs/glass, and Zn NPs/Ti NPs/glass after maintaining for 3 months showed the strong antibacterial activity of 6.1 and 4.3 for *E. coli* and *S. aureus*, respectively. The result shows slightly greater bacterial activity against *E. coli* than that of *S. aureus*, indicating that *S. aureus* has a thicker cell wall compared to *E. coli*.<sup>23</sup> Based on the results, Zn NPs showed a comparable antibacterial effect to silver NPs<sup>24</sup>. The Zn NPs exhibited a strong antibacterial effect although the Zn NPs were maintained in air atmosphere for 3 months. The transmission electron microscopy (TEM) analysis was performed to investigate the variations in crystallinity of the zinc nanoparticle after maintaining in air atmosphere for 3 months. The zinc nanoparticles were directly deposited onto the carbon-coated copper grid for TEM analysis. Figures 7(a) and 7(c) showed the TEM image of the as-deposited zinc nanoparticles and of the Zn particles which were maintained for 3 months, respectively. The lower inset of Fig. 7(a) showed the high-resolution image of the particle within the selected square area, indicating a clear crystallinity of the Zn NP. Figure 7(b) showed the digital diffraction pattern (DDP) obtained by fast Fourier transform (FFT) process from the selected square area (red color) in Fig. 7(a). The DDP showed a clear spot pattern corresponding to <0001> diffraction pattern from the zinc nanoparticle, where (-i100), (01i0), (10i0) spots with an interplanar distance of  $d = 0.28$  nm were marked. On the other hand, as shown in Fig. 7(d), the DDP obtained by FFT from the selected square area in Fig. 7(c) showed an amorphous pattern, which implied the amorphous phase of the nanoparticle. The crystalline zinc nanoparticle was changed to the amorphous phase by an oxidation of the Zn nanoparticles in air atmosphere. Based on the strong antibacterial activity of the Zn NPs maintained for 3 months in air atmosphere (Fig. 6(b)), Zn NPs definitely showed the long-term stability without the protection layer to prevent the oxidation of the zinc NPs in air atmosphere. In order to investigate the actual phase of as-grown Zn NPs and Zn NPs maintained for 3 months in air atmosphere, X-ray photoelectron spectroscopic analysis was performed after surface etching for 10 s to remove the surface contaminations. Figure 7(e) showed the XPS Zn 2P core level of the Zn NPs and Zn NPs maintained for 3 months in air atmosphere. The binding energies of the Zn metal and the ZnO phase in XPS Zn 2P core level were reported as 1021.7 and 1022.2 eV, respectively<sup>25</sup>. Based on the present XPS analysis, as grown Zn NPs are identified as Zn metal, and Zn NPs maintained for 3 months under air atmosphere are remarkably changed to ZnO phase. These results were consistent with the TEM analysis. Figure 7(f) showed the variations in transmittance of the as-deposited and the Zn NPs maintained in air ambient for 3 months. Although the zinc NPs were maintained for 3 months, their transmittance was not changed and was comparable to that of the bare-glass and the as-deposited zinc NPs. As a result, zinc NPs deposited onto the glass substrate showed long-term stability for both the antibacterial effect and the transmittance.

In summary, dense and homogeneous zinc NPs deposited on the glass substrate by dc sputtering were investigated for the transmittance, mechanical durability, and antibacterial effect for the glass

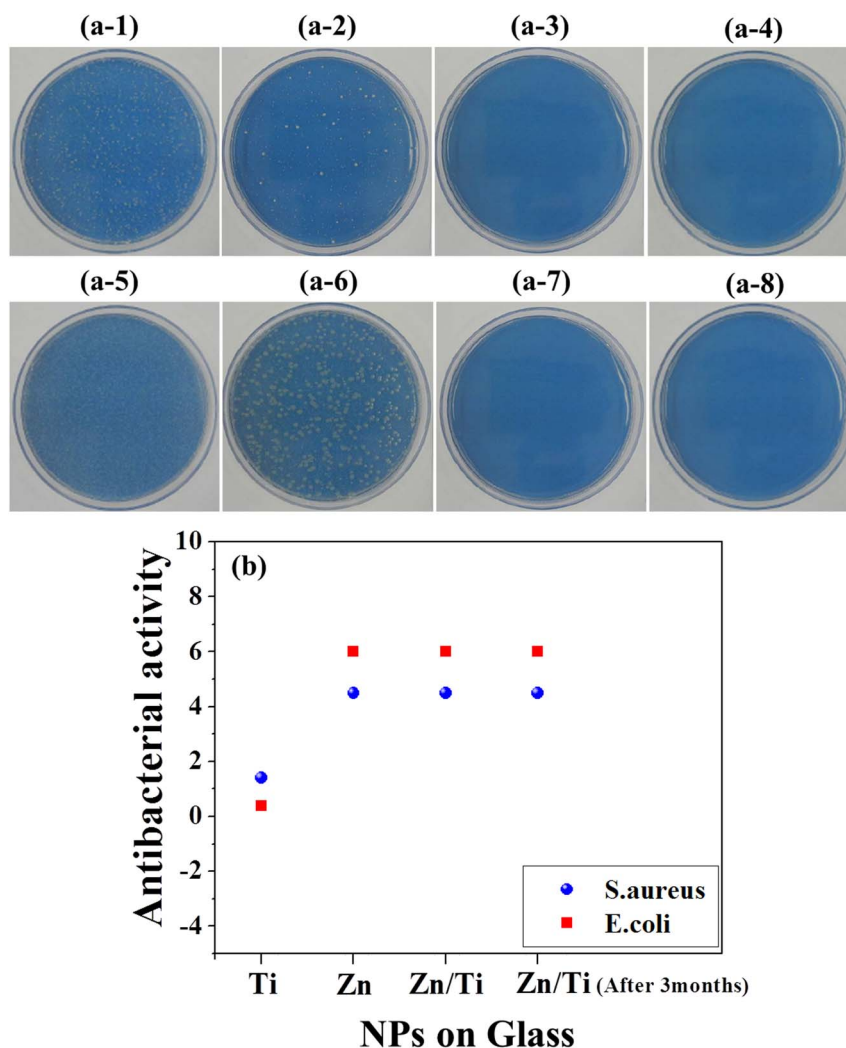


**Figure 6** | Actual images of the incubated (a-1, a-2, a-3, a-4) *S. aureus* and (a-5, a-6, a-7, a-8) *E. coli* bacteria without zinc-NPs (blank), Ti NPs/glass, Zn NPs/SiO<sub>2</sub>/glass, and Zn NPs/Ti NPs/glass, respectively. (b) Antibacterial activities of the Ti NPs/glass, Zn NPs/SiO<sub>2</sub>/glass, Zn NPs/Ti NPs/glass, and Zn NPs/Ti NPs/glass measured after maintaining at 3 months under an air atmosphere at room temperature.

panels of the electronic devices. The buffered Ti NPs were deposited on the glass substrate for a strong adhesion between Zn NPs and glass substrate. The Zn NPs grown on the Ti NPs/glass showed a high

transmittance of approximately 91.5% at a wavelength of 550 nm and a strong antibacterial activity. The Zn NPs/Ti NPs/glass showed a good mechanical durability by the 2,000 repeated swipes. The

**Table 1** | Antibacterial test results after 24 h incubation against *S. aureus* and *E. coli* using samples of Ti NPs/glass, Zn/SiO<sub>2</sub>/glass, Zn NPs/Ti NPs/glass, and Zn NPs/Ti NPs/glass maintained at room temperature in air atmosphere for 3 months

Sample	Bacteria	Case	Start (cells/cm <sup>2</sup> )	After 24 h (cells/cm <sup>2</sup> )	Reduction of Bacteria (%)
<b>Ti</b>	<i>E. coli</i>	Blank	$1.3 \times 10^4$	$6.3 \times 10^5$	-
		Coating film	$1.3 \times 10^4$	$2.8 \times 10^5$	-
	<i>S. aureus</i>	Blank	$1.4 \times 10^4$	$1.9 \times 10^4$	-
		Coating film	$1.4 \times 10^4$	$8.1 \times 10^2$	94.2
<b>Zn</b>	<i>E. coli</i>	Blank	$1.3 \times 10^4$	$6.3 \times 10^6$	-
		Coating film	$1.3 \times 10^4$	<0.63	99.99999
	<i>S. aureus</i>	Blank	$1.4 \times 10^4$	$1.9 \times 10^4$	-
		Coating film	$1.4 \times 10^4$	<0.63	99.99668
<b>Zn/Ti</b>	<i>E. coli</i>	Blank	$1.1 \times 10^4$	$6.3 \times 10^6$	-
		Coating film	$1.1 \times 10^4$	<0.63	99.99999
	<i>S. aureus</i>	Blank	$1.1 \times 10^4$	$1.9 \times 10^4$	-
		Coating film	$1.1 \times 10^4$	<0.63	99.99668
<b>Zn/Ti (After 3 month)</b>	<i>E. coli</i>	Blank	$1.1 \times 10^4$	$1.4 \times 10^6$	-
		Coating film	$1.1 \times 10^4$	<0.63	99.99999
	<i>S. aureus</i>	Blank	$1.2 \times 10^4$	$3.4 \times 10^4$	-
		Coating film	$1.2 \times 10^4$	<0.63	99.99668

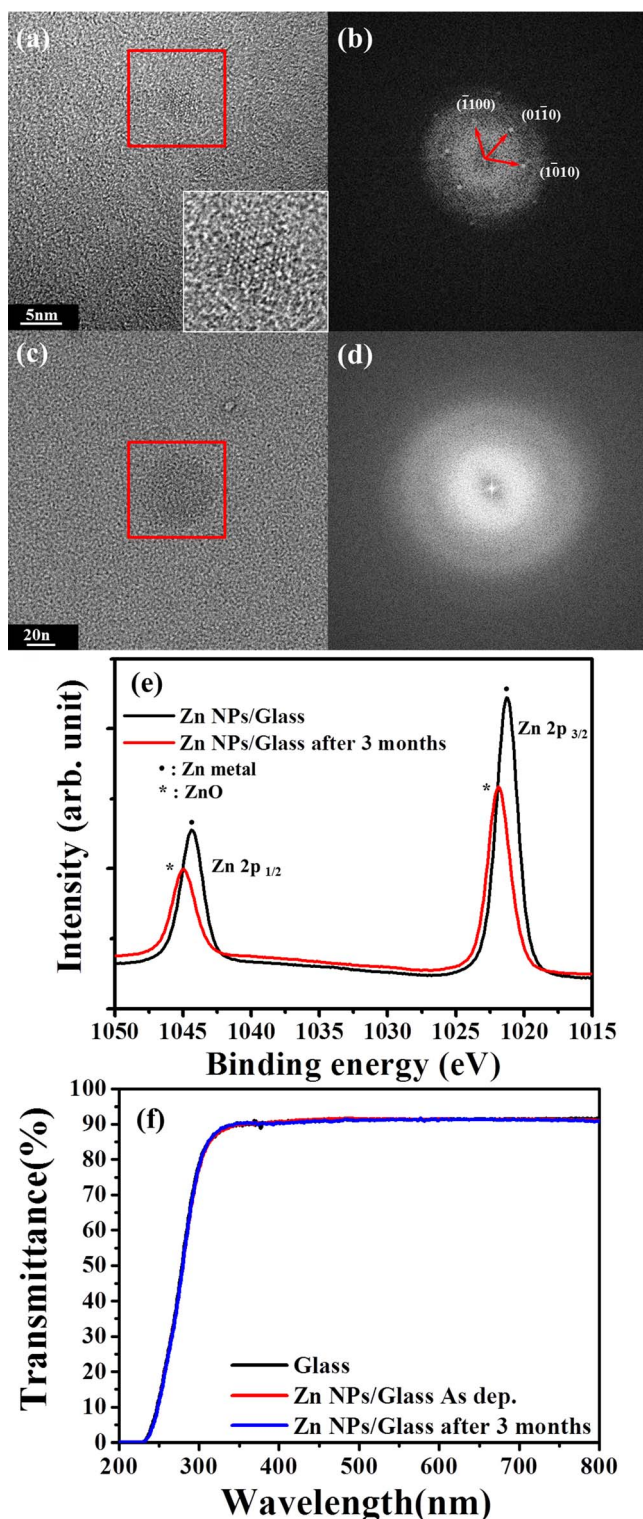


**Figure 7** | TEM image of the (a) as-deposited zinc nanoparticle and of the (c) particle which maintained for 3 months. (b) and (d), the DDP obtained by FFT from the selected areas in (a) and (c), respectively. (e) XPS Zn 2P core levels of as-grown Zn NPs and Zn NPs maintained for 3 months in air atmosphere. (f) Variations in transmittance of the bare-glass substrate, as-deposited Zn particle, and the Zn NPs maintained for 3 months at room temperature in air atmosphere.

buffered Ti NPs are attractive for the enhanced transparent and the strong antibacterial Zn NPs with a mechanical endurance. The Zn NPs did not require the protection layer to prevent the degradation of both the antibacterial effect and the transmittance.

## Methods

The 15 nm-thick SiO<sub>2</sub> buffered films, for a strong attachment of the Zn NPs with the glass substrate (4.5 × 4.5 cm<sup>2</sup>), were deposited via rf magnetron sputtering using a SiO<sub>2</sub> quartz target (purity of 99.99%) with a diameter of 2 in. onto the reinforced (Corning Gorilla) glass substrates. Their deposition was performed under conditions such as a deposition rate of about 1 nm/min, a working pressure of 0.13 Pa, an argon flow rate of 20 sccm (standard cc min<sup>-1</sup>), and an rf power of 100 W. Ti NPs as the buffer layer were deposited onto the glass substrate using Ti metal target (purity of 99.99%) with a diameter of 2 in. under the conditions of dc power of 20 W for 40 s. The Zn NPs by a zinc target (purity of 99.99%) 2 in. in diameter were *in situ* prepared on the 15 nm-thick SiO<sub>2</sub> films and Ti NPs, respectively, for 10 s at a dc power of 6 W under a working pressure of 0.13 Pa without breaking a vacuum.

The optical properties (transmittance) of the zinc NPs/glass with and without buffer layers were investigated using an HP 8453 UV-VIS spectrophotometer. The surface image and the roughness of zinc NPs were observed using field-emission scanning electron microscopy (FE-SEM, Sirion, FEI (Netherlands)) and atomic force microscopy (AFM, Auto Probe CP). Sheet resistances of zinc NPs were measured using a four-point probe method. The crystallinity and elemental analysis of the as-deposited Zn NPs and of the Zn NPs which were maintained at room temperature in air atmosphere for 3 months was investigated using transmission electron microscopy (TEM, Tecnai TF30 ST) and X-ray photoelectron spectroscopy (XPS, ThermoScientific K-Alpha), respectively. The Zn NPs for TEM analysis were deposited onto the carbon-coated copper grid.

An antibacterial test was performed at the FITI testing & Research Institute (Korea) using the film-attachment method<sup>20</sup>. The following microorganisms were used: *Staphylococcus aureus* strain, American Type Culture Collection No. 6538, which is Gram-positive; *Escherichia coli*, American type Culture Collection No. 8739, which is Gram-negative. Blank experiment was carried out using uncoated glass. The test conditions were performed by calculating the number of bacteria after incubation at 35 ± 1 °C for 24 h using an RH 90% solution. The concentration of the surviving bacteria was determined at this time. The conditions of detailed experiments were described at JIS Z 2801<sup>20</sup>.

Mechanical durability of the zinc NPs/glass was tested through the swipes only. The sample size for the swipes was approximately 4.5 × 4.5 cm<sup>2</sup>. Because the Zn NPs were vertically grown onto the glass substrate, swipes were expected to give the severer damage than the touches. Samples were swiped by a piece of glass with 7.8 cm in width, 11.3 cm in length, and 2.8 cm in height. The impact conditions of the mechanical touch test using the glass were approximately 1.85 × 10<sup>-3</sup> N · m, which placed them within the range of both finger (1.10 × 10<sup>-3</sup> N · m) and pen (2.50 × 10<sup>-3</sup> N · m)<sup>26</sup>.

- Song, K. C., Lee, S. M., Park, T. S. & Lee, B. S. Preparation of colloidal silver nanoparticles by chemical reduction method. *Kor. J. Chem. Eng.* **26**, 153–155 (2009).
- Kang, H. Y., Jung, M. J. & Jeong, Y. K. Antibacterial activity and the stability of an Ag<sup>+</sup> solution made using metallic silver. *Kor. J. Biotechnol. Bioeng.* **15**, 521–524 (2000).
- Burrell, R. E. A scientific perspective on the use of topical silver preparations. *Ostomy/Wound Manage.* **49**, 19–24 (2003).
- Feng, Q. L. *et al.* A mechanistic study of the anti-bacterial effect of silver ions on *Escherichia coli* and *Staphylococcus aureus*. *J. Biomed. Mater. Res.* **52**, 662–668 (2000).
- Hollinger, M. A. Toxicological aspects of topical silver pharmaceuticals. *Crit. Rev. Toxicol.* **26**, 255–260 (1996).
- Ratte, H. T. Bioaccumulation and toxicity of silver compounds: A Review. *Environ. Toxicol. Chem.* **18**, 89–108 (1999).
- Gong, P. *et al.* Preparation and antibacterial activity of Fe<sub>3</sub>O<sub>4</sub>@Ag nanoparticles. *Nanotechnology* **18**, 285604 (2007).
- Navarro, E. *et al.* Toxicity of silver nanoparticles to *Chlamydomonas reinhardtii*. *Environ. Sci. Technol.* **42**, 8959–8564 (2008).
- Loher, S., Schneider, O. D., Maiefisch, T., Bokorny, S. & Stark, W. J. Micro-organism-triggered release of silver nanoparticles from biodegradable oxide carriers allows preparation of self-sterilizing polymer surfaces. *Small* **4**, 824–832 (2008).
- Rosi, N. L. & Mirkin, C. A. Nanostructures in Biodiagnostics. *Chemical Review.* **105**, 1547–1562 (2005).
- Shrivastava, S. & Dash, D. Applying Nanotechnology to Human Health: Revolution in Biomedical Sciences. *Nanotechnology* **18**, 184702 (2007).
- Zhang, Y., Suenaga, K., Collies, C. & Iijima, S. Coaxial Nanocable: Silicon Carbide and Silicon Oxide Sheathed with Boron Nitride and Carbon. *Science* **281**, 973–975 (1998).
- Vayssieres, L., Keis, K., Hagfeldt, A. & Lindquist, S.-E. Three-Dimensional Array of Highly Oriented Crystalline ZnO Microtubes. *Chem. Mater.* **13**, 4395–4398 (2001).
- Ahn, J. S., Hammond, P. T., Rubner, M. F. & Lee, I. Self-assembled particle monolayers on polyelectrolyte multilayers: particle size effects on formation, structure, and optical properties. *Colloid. Surface. A: Physicochem. Eng. Aspects* **259**, 45–53 (2005).
- Yu, J., Yu, J. C. & Zhao, X. The effect of SiO<sub>2</sub> addition on the grain size and photocatalytic activity of TiO<sub>2</sub> thin films. *J. Sol-Gel Sci. Techn.* **24**, 95–103 (2002).





16. Kim, G. S. *et al.* Effects of the thickness of Ti buffer layer on the mechanical properties of TiN coatings. *Surface and Coatings Technol.* **171**, 83–90 (2003).
17. Song, H. S. *et al.* Relationship between Gilbert damping and magneto-crystalline anisotropy in a Ti-buffered Co/Ni multilayer system. *Appl. Phys. Lett.* **103**, 022406–022408 (2013).
18. Zeng, X. Q. *et al.* Hydrogen responses of ultrathin Pd films and nanowire networks with a Ti buffer layer. *J. Mater. Sci.* **47**, 6647–6651 (2012).
19. Brandes, E. A. *Smithells Metals Reference Book*. (Butterworths, London, 1983).
20. Hiroki, K. *et al.* *Antimicrobial Products-Test for Antimicrobial Activity and Efficacy: JIS Z 2801*. (Japanese Standards Association, Tokyo, 2000).
21. Allion, A., Van Hecke, B., Boubetra, A. & Lenestour, F. Methodological approach of antibacterial surfaces characterization. *La Metallurgia Italiana* **1**, 29–34 (2012).
22. Lee, S. M., Lee, B. S., Byun, T. G. & Song, K. C. Preparation and antibacterial activity of silver-doped organic–inorganic hybrid coatings on glass substrates. *Colloid. Surface. A: Physicochem. Eng. Aspects* **355**, 167–171 (2010).
23. Kim, J. S. Antibacterial Activity of Ag<sup>+</sup> Ion-Containing Silver Nanoparticles Prepared Using the Alcohol Reduction Method. *J. Ind. Eng. Chem.* **13**, 718–722 (2007).
24. Heo, S. Y., Park, B. J., Jeong, J. R. & Yoon, S. G. Enhanced transmittance, mechanical durability, and anti-fingerprinting qualities of silver nanoparticles deposited onto glass substrates. *J. Alloy. Compd.* **602**, 255–260 (2014).
25. Moulder, J. F., Stickle, W. F., Sobol, P. E. & Bomben, K. D. *Handbook of X-ray Photoelectron Spectroscopy*. (Physical Electronics, Inc., Minnesota, 1995).
26. Kim, J. W. *et al.* *INO 5R Resistive Touch-Screen Specifications*. (Inotouch Technology Co. Ltd., Korea, 2003).

## Acknowledgments

This work was supported by a National Research Foundation of Korea (NRF) grant funded by the Korean government (MSIP) (No. NRF-2013R1A4A1069528). Ki-Seok An and Min

Wook Jung were supported by a grant (2011-0031636) from the Center for Advanced Soft Electronics under the Global Frontier Research Program of the Ministry of Science, ICT and Future Planning, Korea.

## Author contributions

All authors reviewed the manuscript. H.C., B.P., J.E. and S.H. experimented, analyzed the data, and prepared figures 1–6. J.C. performed the TEM analysis and prepared figure 7. M.J. and K.A. analyzed using XPS and prepared figure 7. S.Y. designed experiments, analyzed the data and wrote the paper.

## Additional information

**Supplementary information** accompanies this paper at <http://www.nature.com/scientificreports>

**Competing financial interests:** The authors declare no competing financial interests.

**How to cite this article:** Choi, H.-J. *et al.* Enhanced transparency, mechanical durability, and antibacterial activity of zinc nanoparticles on glass substrate. *Sci. Rep.* **4**, 6271; DOI:10.1038/srep06271 (2014).



This work is licensed under a Creative Commons Attribution-NonCommercial-NoDerivs 4.0 International License. The images or other third party material in this article are included in the article's Creative Commons license, unless indicated otherwise in the credit line; if the material is not included under the Creative Commons license, users will need to obtain permission from the license holder in order to reproduce the material. To view a copy of this license, visit <http://creativecommons.org/licenses/by-nc-nd/4.0/>